Energy Conversion and Management 208 (2020) 112574

Contents lists available at ScienceDirect

Energy Conversion and Management

journal homepage: www.elsevier.com/locate/enconman

Experimental study on transcritical Rankine cycle (TRC) using CO_2/R134a mixtures with various composition ratios for waste heat recovery from diesel engines

Peng Liu[a,b], Gequn Shu[a,*], Hua Tian[a,*], Wei Feng[b], Lingfeng Shi[c], Xuan Wang[a]

[a] State Key Laboratory of Engines, Tianjin University, 92 Weijin Road, Nankai District, Tianjin 300072, China
[b] Energy Technologies Area, Lawrence Berkeley National Laboratory, 1 Cyclotron Road, Berkeley, CA 94720, USA
[c] Department of Thermal Science and Energy Engineering, University of Science and Technology of China, Hefei 230027, China

ARTICLE INFO

Keywords:
CO_2 based mixtures
Transcritical Rankine cycle (TRC)
Composition ratio
Heat transfer performance
Engine waste heat recovery

ABSTRACT

A carbon dioxide (CO_2) based mixture was investigated as a promising solution to improve system performance and expand the condensation temperature range of a CO_2 transcritical Rankine cycle (C-TRC). An experimental study of TRC using CO_2/R134a mixtures was performed to recover waste heat of engine coolant and exhaust gas from a heavy-duty diesel engine. The main purpose of this study was to investigate experimentally the effect of the composition ratio of CO_2/R134a mixtures on system performance. Four CO_2/R134a mixtures with mass composition ratios of 0.85/0.15, 0.7/0.3, 0.6/0.4 and 0.4/0.6 were selected. The high temperature working fluid was expanded through an expansion valve and then no power was produced. Thus, current research focused on the analysis of measured operating parameters and heat exchanger performance. Heat transfer coefficients of various heat exchangers using supercritical CO_2/R134a mixtures were provided and discussed. These data may provide useful reference for cycle optimization and heat exchanger design in application of CO_2 mixtures. Finally, the potential of power output was estimated numerically. Assuming an expander efficiency of 0.7, the maximum estimations of net power output using CO_2/R134a (0.85/0.15), CO_2/R134a (0.7/0.3), CO_2/R134a (0.6/0.4) and CO_2/R134a (0.4/0.6) are 5.07 kW, 5.45 kW, 5.30 kW, and 4.41 kW, respectively. Along with the increase of R134a composition, the estimation of net power output, thermal efficiency and exergy efficiency increased at first and then decreased. CO_2/R134a (0.7/0.3) achieved the maximum net power output at a high expansion inlet pressure, while CO_2/R134a (0.6/0.4) behaves better at low pressure.

1. Introduction

Heavy-duty trucks are one of the main consumers of fossil fuel. In China, heavy trucks, which account for 13.9% of vehicles, consume 49.2% of the total fuel consumed by transport. It is expected that by 2040, heavy-duty trucks will become the largest contributor of carbon dioxide (CO_2) emissions in the transport sector [1]. China and United States are the two largest markets for commercial vehicles in the world. In 2017, China and the United States jointly launched a five-year research in the field of commercial trucks. This program aims to demonstrate technical solutions that could achieve a goal of increasing truck efficiency by 50% over a 2016 baseline. In this program, waste heat recovery (WHR) technology by means of thermodynamic cycles, including Organic Rankine cycle (ORC) and non-organic power cycle, is considered as a promising solution to achieve this goal [2].

Extensive theoretical studies have been involved in ORC-WHR for waste heat recovery from heavy-duty diesel (HDD) engines [3–5]. Recently, several researchers and vehicle manufacturers have developed ORC prototypes, which have been tested in the laboratory and on-road vehicles [6–8]. Alshammari et al. [6] evaluated the potential of fuel efficiency improvement of an ORC prototype for an HDD engine using R245fa and Fluid A as working fluids. Guillaume et al. [9] experimentally discussed the possibility of R1233ze as substitute of R245fa for ORC-WHR on truck applications. AVL [10] presented the results of ORC-WHR for a long-haul truck from test bench and public road testing and indicated that fuel consumption benefits for different real-life cycles in the United States and Europe reach between 2.5% and 3.4%. Cummins [7] has installed an ORC prototype (R245fa as working fluid) on a heavy-duty truck, and the test results showed that brake thermal efficiency of diesel engine increased by 3.6%. Although refrigerants as working fluids of ORC is promising in terms of fuel efficiency improvement, there are still some drawbacks for them in high-

* Corresponding authors.
E-mail addresses: sgq@tju.edu.cn (G. Shu), thtju@tju.edu.cn (H. Tian).

https://doi.org/10.1016/j.enconman.2020.112574
Received 20 October 2019; Received in revised form 10 January 2020; Accepted 1 February 2020
Available online 18 February 2020
0196-8904/

Nomenclature

A	Area (m^2)
c_p	Specific heat (kJ/kW K)
E	Exergy flow rate (kW)
h	Enthalpy (kJ/kg)
HTC	Heat transfer coefficient (W/m^2 °C)
I	Exergy destruction (kW)
m	Mass flow rate (kg/s)
P	Pressure (MPa)
s	Entropy (kJ/kg K)
Q	Heat flow rate (kW)
T	Temperature (°C)
W	Power output (kW)
η	Efficiency (%)
ΔT_{lm}	Log mean temperature difference (°C)

Subscripts

1–8	State point
ave	Average
con	Condenser
cw	Cooling water side
eg	Exhaust gas side
ex	Exergy
exp	Expansion process
est	Estimate
gh	Gas heater
HP	High pressure
is	Isentropic
in	Inlet
LP	Low pressure
max	Maximum
net	Net power
out	Outlet
p	Pump
pre	Preheater
reg	Regenerator
t	Turbine
th	Thermal
wf	Working fluid

Abbreviations

CW	Cooling water
C-TRC	CO_2 Transcritical Rankine Cycle
EC	Engine coolant
EG	Exhaust gas
GH	Gas heater
ICE	Internal combustion engine
PRE	Preheater
REG	Regenerator
RD	Relative difference
R-TRC	Regenerative Transcritical Rankine Cycle
TRC	Transcritical Rankine Cycle
WHR	Waste heat recovery

temperature ORC field, including low thermal decomposition temperature, unsatisfied thermo-economic performance and relatively high ozone depletion potential (ODP) and global warming potential (GWP).

Compared with subcritical Rankine cycle (SRC), transcritical Rankine cycle (TRC) has been proven to achieve better thermal matching and exergy efficiency [3,11]. Previous studies by our group [3] compared the SRC and TRC for diesel engine waste heat recovery, concluding that TRC could obtains a 5.4% increase in thermal efficiency. Yang et al. [12,13] proposed a TRC to recover waste heat from marine diesel engine and compared economic performance of TRCs using various working fluid. Yağlı et al. [14] designed SRC and TRC for waste heat recovery from biogas fueled combined heat and power engine, indicating that the net power output of TRC is higher than that of SRC by 2.9%.

Nowadays, CO_2 transcritical Rankine cycle (C-TRC) has been drawing more and more attention as an application in the waste heat recovery field. The main advantages of using CO_2 as working fluid are desirable thermodynamic performance [15], small size with compact heat exchangers [16,17] and turbines [18], and outstanding environmental performance with zero ODP and extremely low GWP. Specific to WHR from a diesel engine, C-TRC is also beneficial for simultaneous utilization of high and low temperature waste heat sources [19] and presents a good dynamic characteristic [20]. Several prior research studies have discussed and demonstrated the potential of C-TRC for diesel engine [21–23]. Shu's group [24] has proposed a C-TRC prototype to recover exhaust gas and engine coolant waste heat from a heavy duty diesel engine. Experimental results indicated that thermal efficiency of the studied diesel engine could be increased from 39.4% to 41.4% by such WHR system. However, due to low critical temperature of CO_2, the application of C-TRC, especially for WHR from diesel engine, faced the challenge of low-temperature condensation. In addition, the cycle efficiency of C-TRC is relatively low due to its high expansion outlet pressure.

To overcome these disadvantages, CO_2 based mixtures, composed of CO_2 and a chemical with high critical temperature, were investigated in solar plants [25,26], geothermal plants [27,28] and WHR plants [29,30]. Manzolini et al. [25] discussed the potential of a CO_2 mixture in improving thermodynamic and thermo-economic performance for a solar power plant, indicating that the CO_2 mixture outperformed pure CO_2 in conversion efficiency by 2%. Dai et al. [31] studied several CO_2 mixtures in TRC for low temperature heat conversion, demonstrating that CO_2 mixtures are capable of improving thermal efficiency and decreasing operating pressure. Shu et al. [29] considered CO_2 mixtures as working fluid in TRC for diesel engine WHR and concluded that CO_2 mixtures can help expand condensation pressure range. The same conclusions were also drawn in Wu et al. [27].

Identifying a proper mixture composition ratio is essential to optimize the thermodynamic performance of a power system. Thus, the effect of composition ratio was fully considered and discussed in previous theoretical research studies. The majority of previous studies looked at the optimal composition ratio of mixtures using thermodynamic analysis with various criterions, such as net power output [32], exergy performance [30] and economic performance [29,33]. Generally, mixtures only with an appropriate composition ratio behave better than their pure-component counterparts [34,35]. Optimization methods, including generic algorithms [36], sequential quadratic programming [37], mixed-integer nonlinear programming [38] and stochastic optimization [39] also were adopted to determine the optimal composition ratio. computer-aided molecular design (CAMD) also has been used to design and identify the composition ratio of mixture [40].

Indeed, these theoretical analysis can help gain a preliminary understanding of the effect of composition ratio on cycle performance, but the conclusive results still need to be obtained by experiment [34]. Published experimental data relating to power cycle using mixtures are extremely rare. A few mixtures, including R234fa/R123 [41], R245fa/R134a [42], R245fa/R152a [43], R245fa/R365mfc [44], R245fa/R600a [45] and R600a/R601a [46], have been investigated by experiment. Existing publications focused on the performance comparison between the mixture and its pure component counterpart. Only one publication by Wang et al. [46] discussed the effect of mixture

composition on cycle performance by experiment. However, the mixtures outlined above were designed for low-temperature application; the application of CO_2 mixtures in high-temperature applications has not yet been experimentally investigated. Furthermore, there are almost no experimental results on the heat transfer coefficient for mixtures within the temperature range of a power cycle [34,35].

Thus, this paper presents the detailed experimental results in a TRC system using CO_2/R134a mixtures with various composition ratios. A regenerative TRC test bench based on an expansion valve was used to recover waste heat of engine coolant and exhaust gas from a heavy-duty diesel engine. With the measured experimental data, the potential of power output was estimated numerically. The main unique contribution of this paper lies in three aspects:

1. Effect of composition ratio of CO_2/R134a mixtures on system performance was investigated by experiment for the first time.
2. Heat transfer coefficients of various heat exchangers using supercritical CO_2/R134a mixtures are provided and discussed, which may give reference for cycle optimization and heat exchanger design for CO_2 mixtures application.
3. Optimal composition ratio of CO_2/R134a mixtures for the maximum net power output, thermal efficiency and exergy efficiency were determined by experiment.

2. CO_2/R134a mixture

Carbon dioxide, as the working fluid for TRC system, is difficult to be condensed at ambient temperature cold source due to its low critical temperature. Hence, CO_2-based mixture is supposed to have a relatively high critical temperature to overcome that issue. Additionally, a CO_2-based mixture should be environmentally friendly and safe, with good thermodynamic performance. R134a is a non-toxic and non-flammable hydrofluorocarbon with insignificant ozone depletion potential (ODP) and a somewhat lower global warming potential (GWP). It is widely used as a replacement to R12. Moreover, R134a is regarded as a high-temperature refrigerant in automobile air conditioners, which also demonstrates the feasibility of using it in an automotive application. Theoretical results in our previous publication [29] showed that CO_2/R134a mixture has moderate temperature glide and could achieve better thermodynamic performance than CO_2/R1234yf and CO_2/R1234ze. Experimental studies have confirmed that a CO_2/R134a mixture can improve system performance and expand the condensation pressure range of C-TRC [47]. To analyze the effect of the composition ratio on system performance, four CO_2/R134a mixtures with various composition ratio were selected for this study. Among them, the mass fractions of CO_2 were 0.85, 0.7, 0.6 and 0.4. Table 1 includes the main thermodynamic properties of CO_2, R134a and their mixtures. Note that the thermodynamic properties of CO_2/R134a mixtures were obtained from REFPROP 9.0. Furthermore, the GWPs of mixtures were calculated by method provided in Ref. [48].

Fig. 1 provides temperature-entropy (*T-s*) diagrams of selected CO_2/R134a mixtures. It shows that the CO_2/R134a mixtures all can be categorized into wet fluid. Critical temperatures of mixtures increase with the mass fraction of R134a. However, critical pressures of CO_2/R134a mixtures are not necessarily lower than pure CO_2, even when adding refrigerant with low critical pressure.

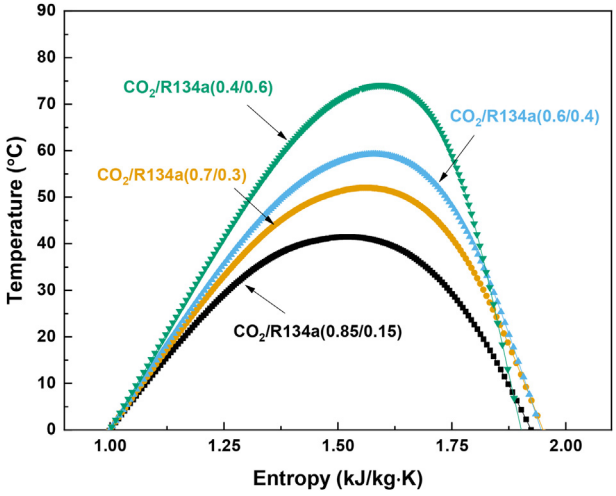

Fig.1. *T-s* diagrams of selected CO_2/R134a mixtures.

3. Experimental facility and methodology

3.1. Experimental test bench

A typical regenerative TRC (R-TRC) test bench was built to recover waste heat of exhaust gas and engine coolant from a diesel engine. Fig. 2 shows the schematic diagram of the whole test bench. The waste heat sources were provided by a six-cylinder, four-stroke heavy-duty diesel engine, equipped with complete measuring and controlling instruments to ensure it operates stably at a specific condition. Its main parameters are listed in Table 2. The cooling water was provided by a refrigeration unit to cool the working fluid in condensers and the working fluid tank. The mass flow rate and temperature of cooling water could be controlled and adjusted.

The R-TRC test bench consists of several heat exchangers, an expansion valve, a plunger pump and a working fluid tank. Table 2 also lists the specification of the main components in the R-TRC test bench. First, CO_2/R134a mixture is pressurized into a supercritical state by the plunger pump. Then the working fluid absorbs heat from the engine coolant, low pressure working fluid after expansion valve and exhaust gas in the preheater, the regenerator and the gas heater, respectively. The high temperature working fluid expands through the expansion valve and flows through the regenerator. Finally, the working fluid is cooled into a liquid state in the condensers. Fig. 3 presents the thermodynamic process of R-TRC using CO_2/R134a mixture in *T-s* diagram.

In the R-TRC test bench, the gas heater was a self-made double-pipe type heat exchanger, while the rest of heat exchangers were commercial plate heat exchangers purchased from SWEP. All heat exchangers and pipes were wrapped by thermal insulation cotton in to reduce heat loss into the environment. The flow rate of the working fluid was controlled and adjusted by a reciprocating plunger pump. The CO_2 expander manufactured for this test bench is still in the test phase. Considering

Table 1
Thermodynamic properties of CO_2, R134a and their mixtures.

	Molecular mass/(g/mol)	T_c /(°C)	P_c/(MPa)	ODP	GWP	ASHRAE 34 safety group
CO_2	44.01	31.1	7.38	0	1	A1
CO_2/R134a (0.85/0.15)	48.11	41.2	7.78	0	206	–
CO_2/R134a (0.7/0.3)	53.06	51.3	7.87	0	412	–
CO_2/R134a (0.6/0.4)	56.97	58.3	7.80	0	549	–
CO_2/R134a (0.4/0.6)	66.80	73.2	7.29	0	822	–
R134a	102.03	101.1	4.06	0	1370	A1

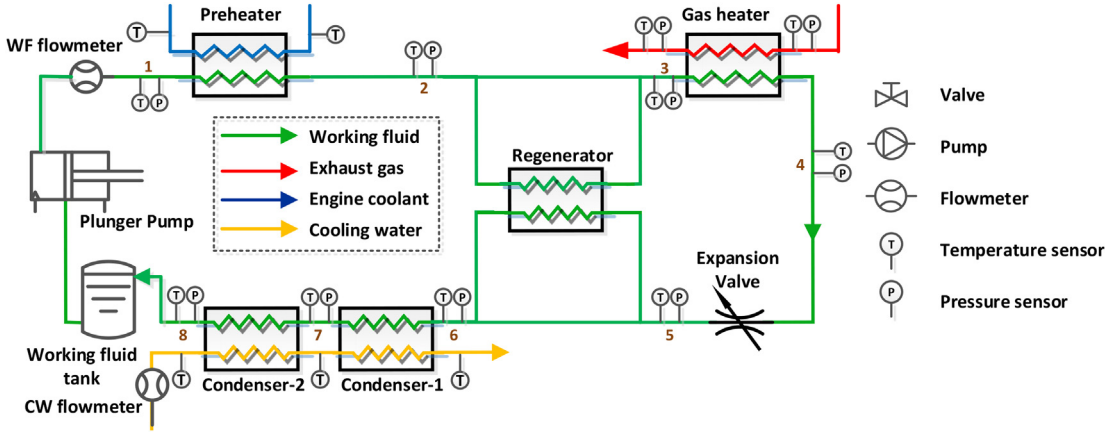

Fig. 2. Diagrams of a preheating regenerative TRC (R-TRC) test bench.

Table 2
Specification summary of the main components.

Heat source	
Diesel engine	Type: Inline type, 6 cylinders Displacement: 8.424 L Rated power: 243 kW Bore × Stroke: 113 mm × 140 mm Maximum torque: 1280 N·m Rated speed: 2200 rpm
ORC system	
Gas heater	Area: 3.09 m^2 Type: Double-pipe type (self-made)
Preheater/Regenerator/Condenser	Area: 1.56 m^2 Type: Brazed plate Flow type: Counter Current Size: 377 mm × 119.5 mm × 92 mm
Expansion Valve	Type: Needle type Opening: 0–100%
Pump	Type: Reciprocating plunger pump Rated flow rate: 1.7 m^3/h Plunger number: 3 Bore × Stroke: 38 mm × 50 mm
Working liquid tank	Type: Vertical cylinder Volume: 10L
Cold source	
Refrigerating unit	Refrigerant: R22 Temperature range: 5 °C–15 °C

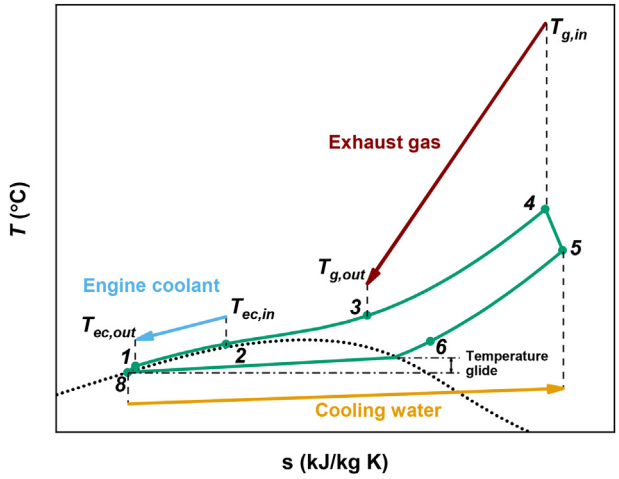

Fig. 3. *T-s* diagrams of the regenerative ORC (R-TRC) using CO_2/R134a mixture.

the possible damage caused by the refrigerant component in CO_2/R134a mixtures, a self-made expansion valve was used to control the system pressures. For the sake of security, the maximum pressure of system cannot exceed 11 MPa and maximum temperature cannot exceed 250 °C. Detailed descriptions and photographs of the R-TRC test bench can be found in our previous publication [47].

3.2. Measurement devices and uncertainty

In addition to the structure of test bench, the position of each measurement point is also indicated in Fig. 2. The thermocouple temperature sensor was installed to measure the temperature of exhaust gas, while the other measurement points used a thermal resistance sensor. Ten pressure transmitters were installed in the test bench to monitor pressures at each measurement point. Hastelloy alloy was used for the pressure sensors in the exhaust side to prevent acid erosion by the exhaust gas. The exhaust gas flow rate was obtained by measuring the intake air flow rate and fuel consumption of the diesel engine. The intake air flow rate was measured by a cylindrical laminar flow meter, while the volume flow rates of the engine coolant and cooling water were measured by a turbine flow meter. A Coriolis type mass flow meter was applied to obtain the precise real-time mass flow rate of the working fluid. Meanwhile, a magnetic flap type fluid level gauge was installed on the working fluid tank to indicate the liquid height. Table 3 lists the measurement range and accuracy of each measurement device.

A data acquisition module was used to acquire and convert signals from measurement devices, and then was connected to the computer via a communication cable. Measured data could be automatically recorded and saved by the second.

After obtaining the measured data, including temperature and pressure, the thermodynamic properties of the working fluid, was

Table 3
Measurement range and accuracy of each measurement device.

Devices	Measurement range/(Accuracy)
Temperature	
Thermocouple sensor	−60–650 °C/(± 1%)
Thermal resistance sensor	−200–500 °C/(± 0.15%)
Pressure	
Exhaust gas side	0–0.5 MPa/(± 0.065%)
High pressure working fluid side	0–14 MPa/(± 0.065%)
Low pressure working fluid side	0–12 MPa/(± 0.065%)
Flow rate	
Working fluid	0–0.3 kg/s/(± 0.2%)
Intake air	0–1350 kg/h/(± 0.5%)
Fuel consumption	5–2000 kg/h/(± 0.8%)
Engine coolant	2–40 m^3/h/(± 0.5%)
Cooling water	0–12 m^3/h/(± 1%)

calculated using the REFPROP 9.0. System uncertainty analysis was conducted using Kline and McClintock method described in our previous publication [20]. The maximum relative uncertainties of heat absorption amount from exhaust gas $Q_{gh,\ wf}$, heat transfer amount in exhaust side $Q_{gh,exh}$, net power output W_{net} and thermal efficiency η_{th} were 1.12%, 5.72%, 1.12% and 2.27% respectively.

3.3. Experimental methodology

The main purpose of this study was to analyze the effect of the composition ratio of CO_2/R134a mixture on R-TRC system performance. Hence, the same external conditions, including heat source and cold source, were imposed in comparative experiments. Previous studies showed that a heavy-duty diesel engine in an automotive application rarely operates at a rated load [49]. Thus, the medium load point of this diesel engine (600 N·m at 1100 rpm) was chosen. Even if the diesel engine operates at a constant speed and torque, it is inevitable that parameters (temperature and flow rate) of exhaust gas, as well as engine coolant, could still fluctuate. Fig. 4 shows the parameter variations of waste heat sources during the experiment. Maximum relative difference RD_{max} is determined by maximum difference between measured value X and average measured value X_{ave} for all experiments, $RD_{max} = (X - X_{ave})_{max}/X_{ave}$. The maximum relative difference of heat source parameters are all less than 10%. Such differences are acceptable in the present comparison experiment.

These experiments were performed at different times with various ambient temperature, and it was difficult to keep an accurate, constant cooling water temperature. Hence, the cooling water temperatures for different experiments are somewhat different. Prior experimental studies have indicated that ambient temperature has a limited impact on system overall performance [41]. Table 4 shows the cooling source conditions of all of the experiments.

Given a constant heat source and cold source condition, all experiments were performed with a working fluid flow rate of 11.5 kg/min. Several sub-scenarios with different pressures in the TRC system could be created by decreasing the opening of the expansion valve. The effect of the composition ratio of the CO_2/R134a mixture on system performance under various pressures was investigated by this experimental strategy. The major indicator for steady state detection of TRC is the expansion inlet pressure, which is a reliable indicator with high accuracy [20]. Fig. 5 depicts the variation of pressures with time. Each step increase of expansion inlet pressure corresponds to a change of expansion valve opening. Several steady operating points for CO_2/R134a mixtures with various pressures were chosen for comparison. These points were obtained after maintaining the TRC system on steady condition for 2–3 min. Pressures of selected steady operating points are summarized in Table 5.

4. Results and discussion

In this section, the experimental results based on the experimental methodology outlined above are presented. The effect of the composition ratio of CO_2/R134a mixture on measured operating parameters, heat exchanger performance and cycle performance was investigated carefully. The difference in the cycle behavior among CO_2/R134a mixtures was explained from the point of thermophysical properties.

Starting with the results of pressure variations shown in Fig. 5 and Table 5, as the mass fraction of R134a increased, expansion outlet pressure P_5 decreased gradually. This effect can be explained by the fact that the CO_2/R134a mixture with a higher fraction of R134a has a lower saturated vapor and liquid pressure at the constant temperature, as shown in Fig. 6. As a direct consequence of that, CO_2/R134a (0.4/0.6) achieved the highest expansion pressure ratio, while CO_2/R134a (0.85/0.15) had the lowest pressure ratio during the expansion process.

Expansion inlet temperature T_4 is an important indicator of power output ability. Fig. 7 depicts the variation of expansion inlet temperature with pressure. As the expansion inlet pressure increased, expansion inlet temperature T_4 climbed from 200.4 °C to 204.6 °C for CO_2/R134a (0.85/0.15), while the opposite trend was presented for CO_2/R134a (0.7/0.3), with a range of 194.8 °C-189.0 °C; and for CO_2/R134a (0.6/0.4), with 183.4 °C −175.2 °C. No sensible change in the T_4 was observed for CO_2/R134a (0.4/0.6) with 192.4 °C-191.6 °C. One factor affecting the behaviors of T_4 is that the decrease of working fluid flow rate, induced by throttle effect in expansion valve, resulted in the rise of T_4 for all four CO_2/R134a mixtures. What's more, the difference of specific heat capacity among various CO_2/R134a mixtures mainly contributed to different trend of T_4.

Fig. 8 shows the variation of specific heat c_p among the various CO_2/R134a mixtures. Before starting this discussion, it should be noted that although there is no phase change process for the supercritical fluid, constant-pressure specific heat would reach a peak at a certain temperature under given pressure. The peak point of specific heat is the pseudocritical point, and its corresponding temperature is the pseudocritical temperature. Looking back at Fig. 1, critical temperatures of CO_2/R134a mixtures increased with the mass fraction of R134a, which also lead to the increase of pseudocritical temperature, as shown in Fig. 8.

For the graphs in Fig. 8, the specific heat c_p curve is divided into three sections, corresponding to heating process in the preheater (A), the regenerator (B) and the gas heater (C). The enclosed area bounded by specific heat c_p curve and X axis indicates the heat absorption amount per mass. Affected by location change of pseudocritical point, the enclosed area of CO_2/R134a mixtures in the exhaust gas recovery zone increases with expansion inlet pressure, indicating lower T_4 would

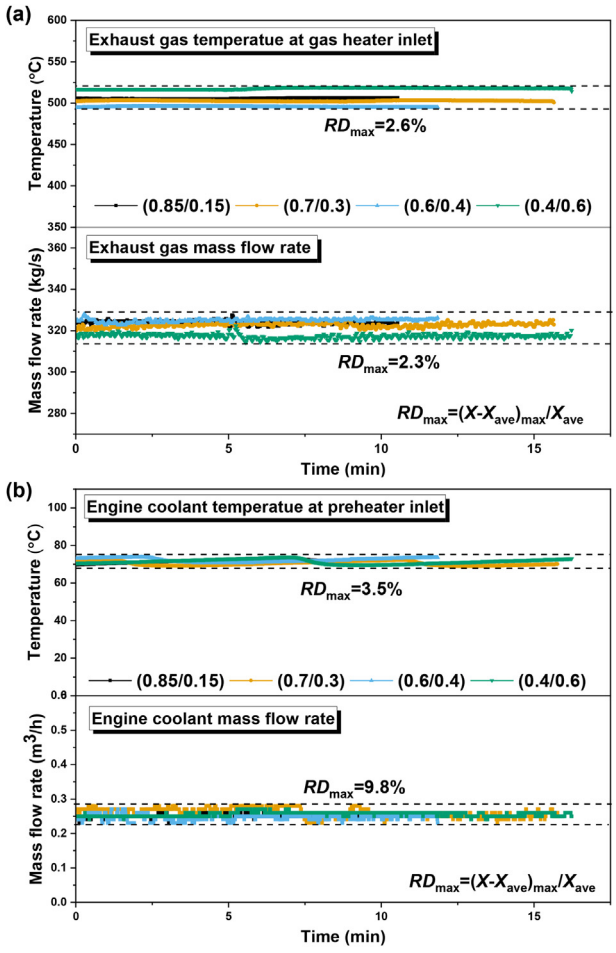

Fig. 4. Parameter variations of waste heat sources during the experiment; (a) exhaust gas; (b) engine coolant.

Table 4
Cooling source conditions.

	CO_2/R134a(0.85/0.15)	CO_2/R134a(0.7/0.3)	CO_2/R134a(0.6/0.4)	CO_2/R134a(0.4/0.6)
Cooling water inlet temperature (°C)	12.8	8.6	9.4	9.2
Cooling water flow rate (m^3/h)	1.98	1.94–1.95	1.91–1.92	1.95–1.96

be obtained by a higher pressure at the same heat absorption amount. This in turn results in a decrease of expansion inlet temperature T_4. Comparing the four CO_2/R134a mixtures, specific heat c_p in the exhaust gas recovery zone increased more in CO_2/R134a (0.7/0.3) and CO_2/R134a (0.6/0.4). Thus, the combined effect of working fluid flow rate variation and specific heat variation may explain the different T_4 trends.

4.1. Heat exchanger performance

For the R-TRC system's heating process, the working fluid flows through the preheater, the regenerator and the gas heater, in sequence. For the cooling process, the working fluid is cooled in two condensers. The performance of these heat exchangers was observed using CO_2/R134a mixtures with different composition ratio. Before starting this discussion, the heat balances of heating process and cooling process were investigated.

In the heating process, the heat absorption amount of working fluid in the preheater, the regenerator and the gas heater could be calculated by Equations (1–3), respectively. While the total heat released by the engine coolant, the low-pressure working fluid after expansion valve and the exhaust gas could be obtained by Eqs. (4–6), respectively.

$$\dot{Q}_{pre,wf} = \dot{m}_{wf}(h_2 - h_1) \quad (1)$$

$$\dot{Q}_{reg,wf,HP} = \dot{m}_{wf}(h_3 - h_2) \quad (2)$$

$$\dot{Q}_{gh,wf} = \dot{m}_{wf}(h_4 - h_3) \quad (3)$$

$$\dot{Q}_{pre,ec} = c_p \dot{m}_{ec}(T_{ec,in} - T_{ec,out}) \quad (4)$$

$$\dot{Q}_{reg,wf,LP} = \dot{m}_{wf}(h_5 - h_6) \quad (5)$$

$$\dot{Q}_{gh,g} = \dot{m}_g(h_{g,in} - h_{g,out}) \quad (6)$$

As for the cooling process, the heat released by the working fluid in condenser 1 and condenser 2 can be estimated by Eq. (7) and (8), while the amount of heat absorbed by the cooling water is calculated using

Table 5
Selected steady operating points for system performance analysis.

	1	2	3	4	5	6	7
CO_2/R134a mixtures (0.85/0.15)							
P_4/(MPa)	7.91	8.79	9.72	10.25	10.78		
P_5/(MPa)	5.55	5.53	5.51	5.50	5.49		
CO_2/R134a mixtures (0.7/0.3)							
P_4/(MPa)	8.04	8.59	9.09	9.66	10.05	10.50	
P_5/(MPa)	4.45	4.45	4.43	4.42	4.41	4.40	
CO_2/R134a mixtures (0.6/0.4)							
P_4/(MPa)	7.90	8.71	9.51	10.08	10.57		
P_5/(MPa)	3.99	3.98	3.97	3.97	3.96		
CO_2/R134a mixtures (0.4/0.6)							
P_4/(MPa)	7.91	8.34	8.84	9.38	9.85	10.27	10.51
P_5/(MPa)	3.85	3.84	3.83	3.80	3.79	3.78	3.77

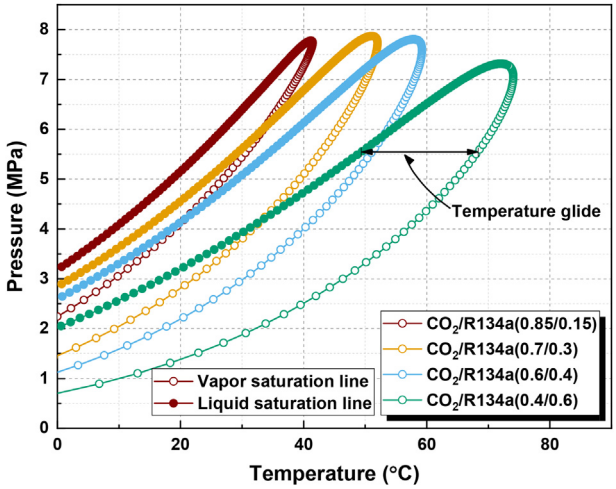

Fig. 6. Saturated vapor and liquid line of CO_2/R134a mixtures.

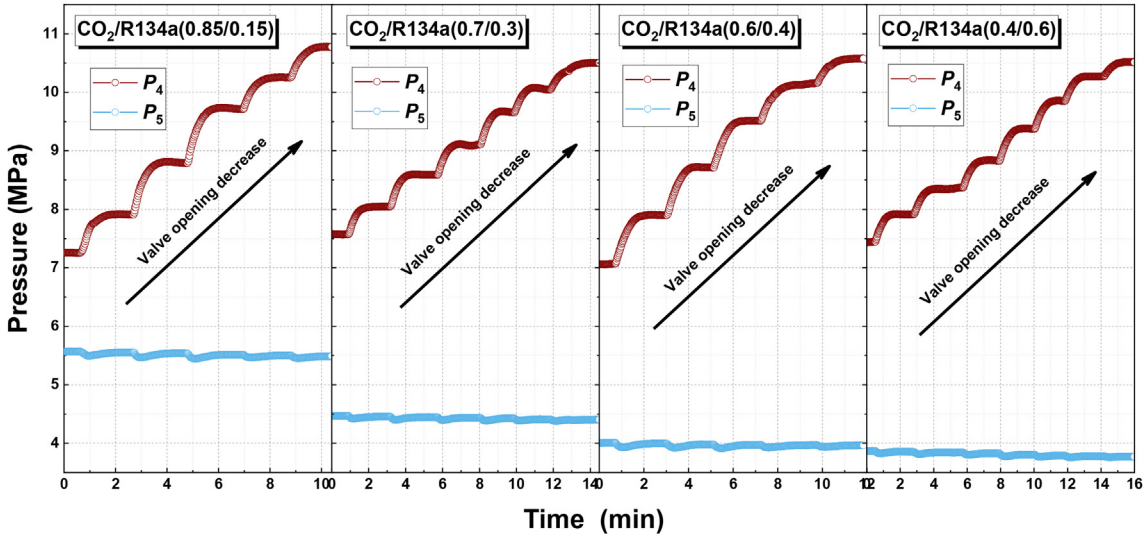

Fig. 5. Variations of pressures with time during the experiment.

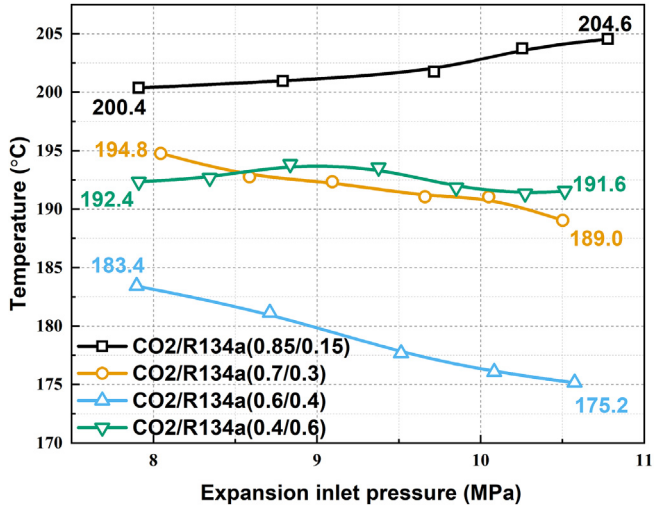

Fig. 7. Variation of expansion inlet temperature with expansion inlet pressure.

Eq. (9) and (10).

$$\dot{Q}_{con1,wf} = \dot{m}_{wf}(h_6 - h_7) \tag{7}$$

$$\dot{Q}_{con2,wf} = \dot{m}_{wf}(h_7 - h_8) \tag{8}$$

$$\dot{Q}_{con1,cw} = \dot{m}_{cw}(h_{cw,out} - h_{cw,m}) \tag{9}$$

$$\dot{Q}_{con2,cw} = \dot{m}_{cw}(h_{cw,m} - h_{cw,in}) \tag{10}$$

Fig. 9 shows the parity plot of the heat flow rate differences between the primary and secondary fluid sides for the heating and cooling processes. The main reason for this disagreement may be attributed to the measuring error and heat loss during the heat transfer process. However, for all cases, the discrepancies of heat flow rate are within 10% in the heating process and 6% in the cooling process. Hence, the heat balances in both the heating and cooling processes are satisfactory, and the measurement data are reliable. In this study, the evaluation of heat exchanger performance and cycle performance was performed based on the heat flow rate absorbed or released by the working fluid.

Fig. 10 depicts the heat absorption amount in the preheater, the regenerator and the gas heater. It is clear that exhaust gas is the main contributor to the amount of total heat absorption. By increasing the mass fraction of R134a in the mixtures, the amount of total heat absorption declined, which was caused mainly by the decrease of the heat absorption amount in the regenerator, as shown in Fig. 10. As mentioned earlier, the CO_2/R134a mixture with a higher fraction of R134a has a higher expansion ratio, leading to a lower expansion outlet temperature. Thus, the amount of heat absorption in the regenerator declined. A further interesting finding was that CO_2/R134a (0.4/0.6) can absorb more heat from the exhaust gas, but less heat from the engine coolant in comparison with the rest of the mixtures. This could be attributed to the difference of specific heat for various CO_2/R134a mixtures, as shown in Fig. 8.

Heat transfer performance of a supercritical fluid is a hot topic that attracts attention from many researchers. Some experimental results about pure CO_2 heat transfer performance in supercritical condition have been reported [50,51]. However, there is little experimental data on the heat transfer coefficient (HTC) of mixtures in the temperature range of the power cycle [35]. Here, the heat transfer performances of various CO_2/R134a mixtures in the preheater, the regenerator and the gas heater are presented and discussed in detail. Fig. 11 depicts the *T-Q* diagram of the heating process for various CO_2/R134a mixtures, based on experimental data. The HTC is estimated as:

$$U = \dot{Q}/A/\Delta T_{lm} \tag{11}$$

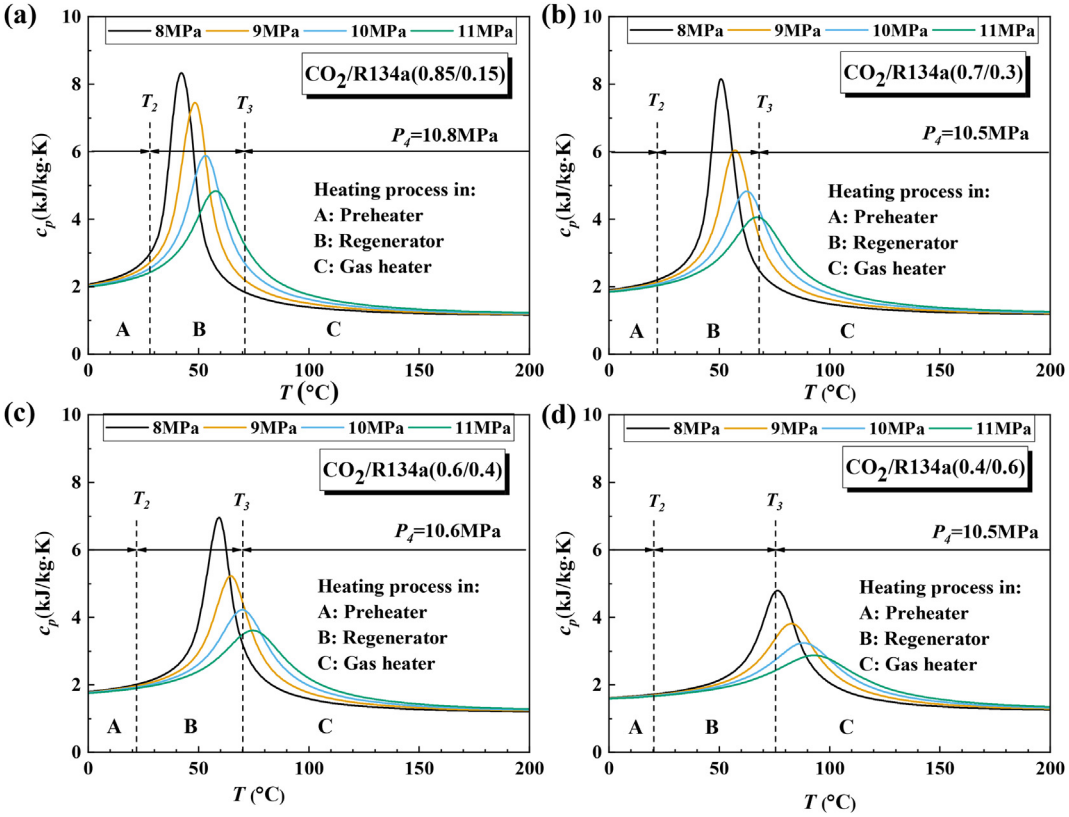

Fig. 8. Variation of specific heat capacity for various CO_2/R134a mixtures: (a) CO_2/R134a (0.85/0.15); (b) CO_2/R134a (0.7/0.3); (c) CO_2/R134a (0.6/0.4); and (d) CO_2/R134a (0.4/0.6).

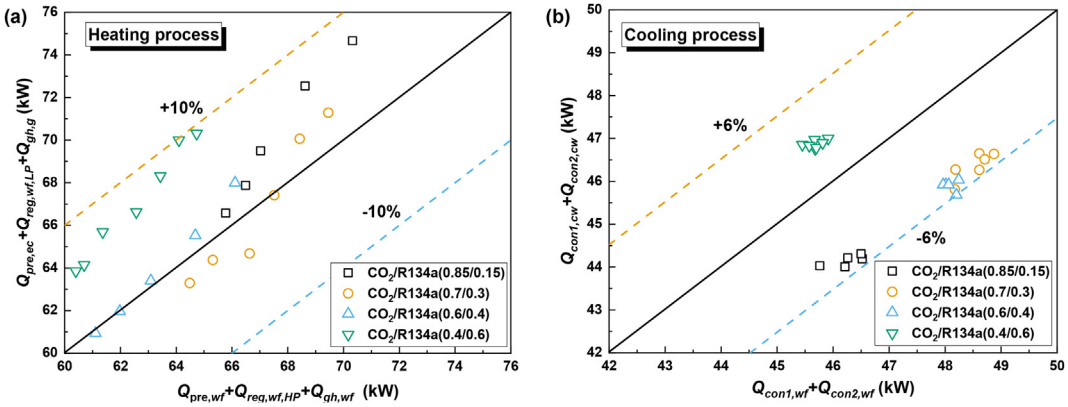

Fig. 9. Heat flow rate in (a) the heating process; (b) the cooling process.

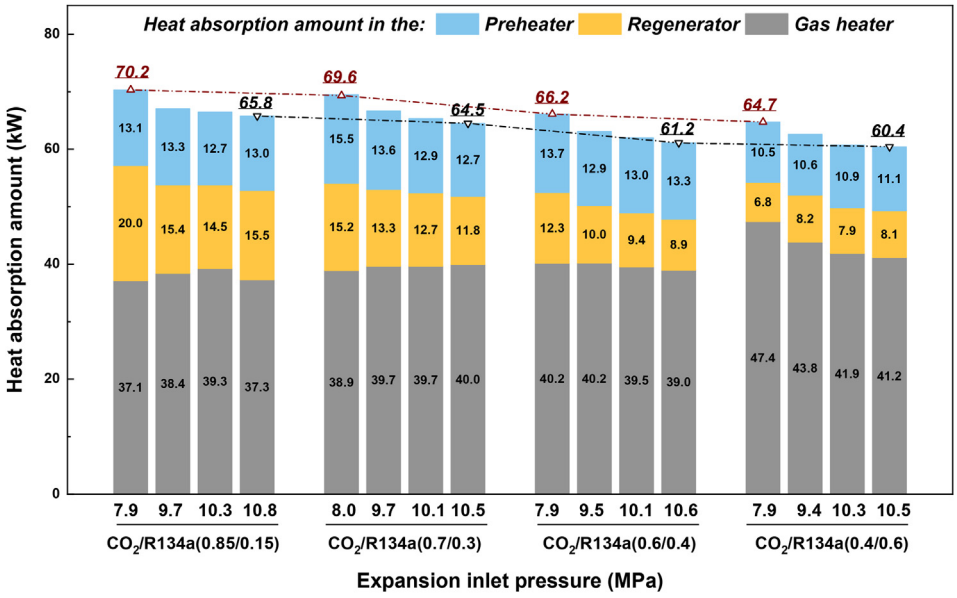

Fig. 10. Heat absorption amount for the various CO_2/R134a mixtures.

wherein $\dot{Q}$ is the heat absorption amount by working fluid, A is the heat transfer area of each heat exchanger provided in Table 2. ΔT_{lm} is the log mean temperature difference. Table 6 shows the overall heat transfer coefficients in various heat exchangers. Based on experimental data in our previous publication [47], heat transfer coefficient of pure CO_2 under supercritical condition in various heat exchanger is also included in Table 6. For CO_2/R134a mixtures, the results showed that the HTCs are in the range of 697.9–1286.7 W/m^2 °C for the preheater, 115.6–164.0 W/m^2 °C for the regenerator, and 107.6–111.7 W/m^2 °C for the gas heater. The HTCs in the preheater are obviously larger than those in the regenerator and the gas heater. These results are reasonable, because the convection heat transfer coefficient in liquid–liquid cases is generally larger than those in liquid–gas cases.

Different thermodynamic properties, induced by the composition ratio in CO_2/R134a mixtures, also influence the overall HTCs. For the supercritical fluid, the specific heat reach peak at the pseudocritical point as shown in Fig. 8, indicating that more heat could be transferred near the pseudocritical point. Meanwhile, density, viscosity and thermal conductivity also sharply decreased in the vicinity of the pseudocritical point, which contributed to the increase in flow velocity. Thus, better heat transfer performance may be achieved near the pseudocritical point [50]. Ma et al. [52] concluded that HTCs of supercritical CO_2 side and overall heat transfer exchanger have similar trends with specific heat for a double pipe heat exchanger. Based on this, for the preheater, the HTC of CO_2/R134a (0.85/0.15) is significantly higher than that of CO_2/R134a (0.4/0.6), while the HTC of CO_2/R134a (0.7/0.3) is similar to that of CO_2/R134a (0.6/0.4). For the regenerator, the HTC of CO_2/R134a (0.4/0.6) is lower than those of other mixtures. As for the gas heater, the difference of heat transfer coefficient among CO2/R134a mixtures is not evident, since the convection heat transfer coefficient in the exhaust gas side is much lower than that in the working fluid side, and the overall heat transfer coefficient depends on the heat transfer performance of the exhaust gas side to a great extent.

4.2. Cycle performance

An experimental comparison of CO_2/R134a mixtures with various composition ratios was performed by discussing the net power output, thermal efficiency and exergy efficiency. Although an expansion valve was used instead of the expander in the test bench to control pressure, it was still possible to estimate numerically the net power output based on experimental results, by assuming constant isentropic expansion efficiency. In the numerical analysis, the experimental data, including expansion inlet pressure, expansion inlet temperature and expansion outlet pressure, was used. The net power output can be estimated as:

$$\dot{W}_{exp,est} = \dot{m}_{wf}(h_4 - h_{5,ideal})\eta_{exp} \quad (12)$$

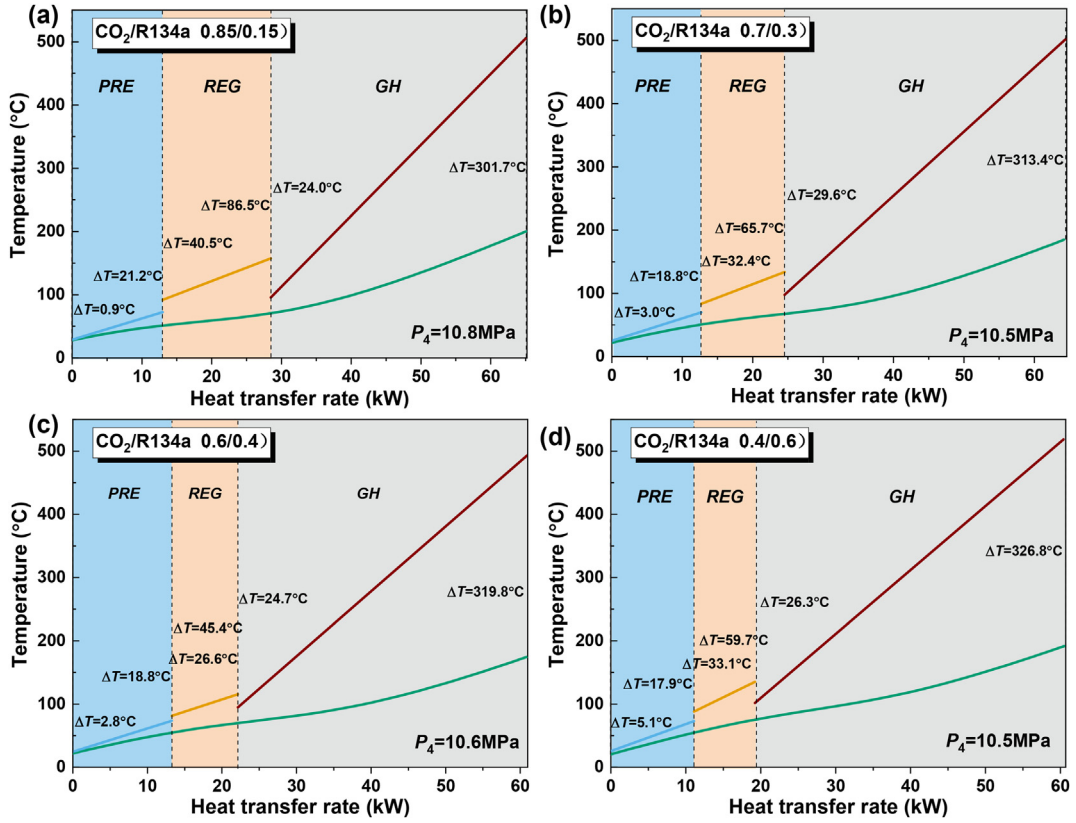

Fig. 11. *T-Q* diagram for heating process for various CO_2/R134a mixtures: (a) CO_2/R134a (0.85/0.15); (b) CO_2/R134a (0.7/0.3); (c) CO_2/R134a (0.6/0.4); and (d) CO_2/R134a (0.4/0.6).

Table 6
Heat transfer coefficients (HTCs) of the preheater, the regenerator and the gas heater for various CO_2/R134a mixtures.

	Pure CO_2	CO_2/R134a (0.85/0.15)	CO_2/R134a (0.7/0.3)	CO_2/R134a (0.6/0.4)	CO_2/R134a (0.4/0.6)
Expansion inlet pressure (MPa)	10.7	10.8	10.5	10.6	10.5
HTC of the preheater (W/m^2 °C)	868	1286.7	947.3	1012.3	697.9
HTC of the regenerator (W/m^2 °C)	169.9	164.0	161.1	161.4	115.9
HTC of the gas heater (W/m^2 °C)	101.3	109.2	107.6	109.6	111.7

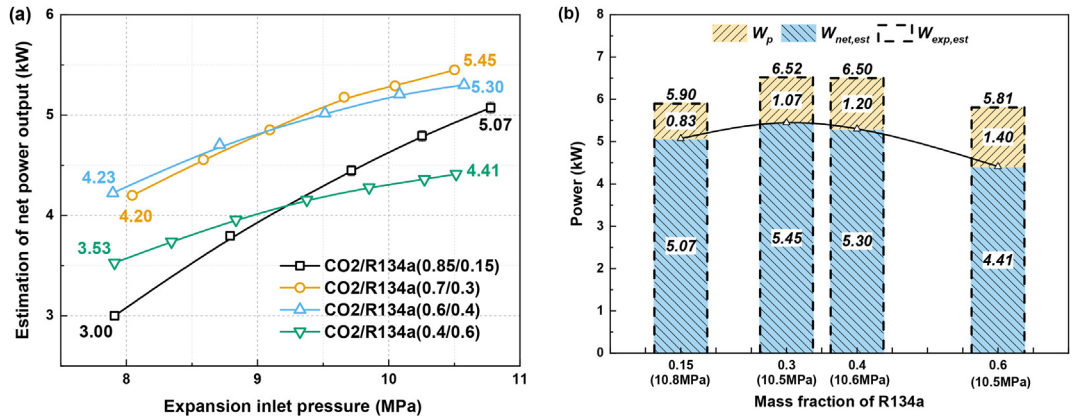

Fig. 12. (a) Estimation of net power output as a function of expansion inlet pressure; (b) Effect of composition ratio on estimation of net power output.

$$\dot{W}_p = \dot{m}_{wf}(h_1 - h_8) \tag{13}$$

$$\dot{W}_{net,est} = \dot{W}_{exp,est} - \dot{W}_p \tag{14}$$

Experimental results of small-scale expanders using CO_2-based mixture are lacking. In this study, the expansion efficiency was set at 70%, which is the target of the CO_2 turbine manufactured for the test bench and also reasonable for currently running CO_2 applications [53].

Fig. 12(a) shows the estimation of net power output for various CO_2/R134a mixtures. For all cases, the estimation of net power output increased with expansion inlet pressure, but the increase rate of CO_2/R134a (0.85/0.15) was higher than those of other mixtures. This

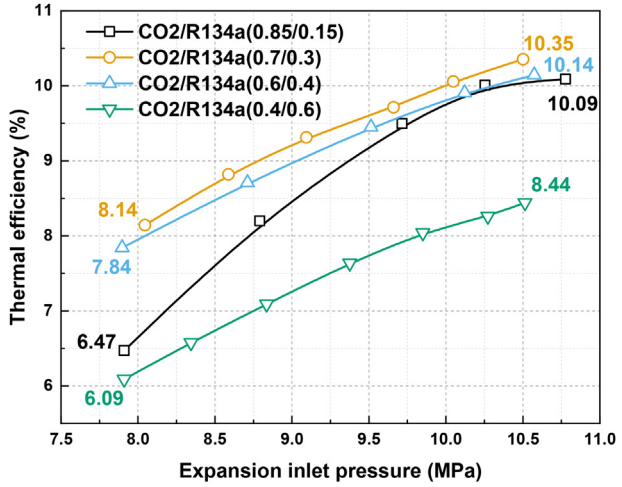

Fig. 13. Thermal efficiency as a function of expansion inlet pressure.

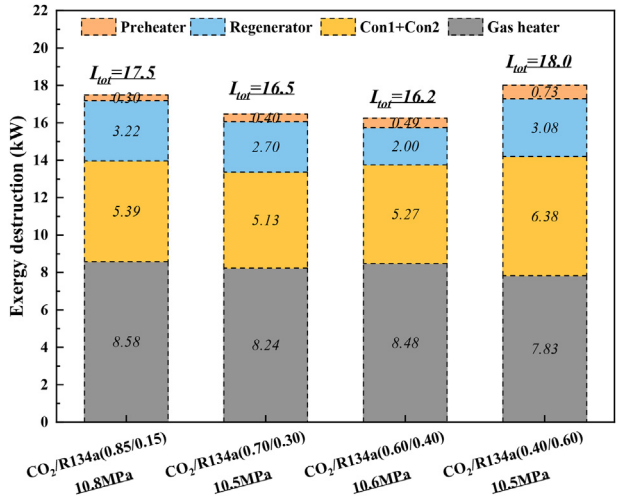

Fig. 14. Exergy destruction comparisons among the various heat exchangers.

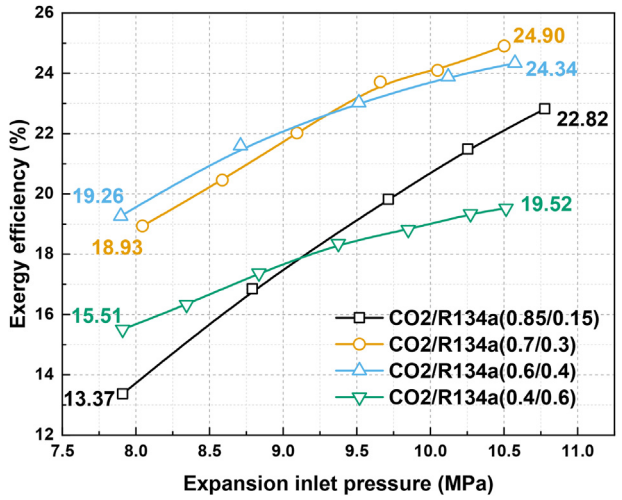

Fig. 15. Exergy efficiency as a function of expansion inlet pressure.

difference may be attributed to the increase of the expansion inlet temperature depicted in Fig. 7. Maximum net power output was achieved by maximizing the expansion inlet pressure in experimental pressure range. Thus, the maximum net power outputs of CO_2/R134a (0.85/0.15), CO_2/R134a (0.7/0.3), CO_2/R134a (0.6/0.4) and CO_2/R134a (0.4/0.6) are 5.07 kW, 5.45 kW, 5.30 kW, and 4.41 kW, respectively.

As for the effect of composition ratio, by increasing the mass fraction of R134a, the net power output increased at first and then declined. At high expansion inlet pressure, CO_2/R134a (0.7/0.3) achieved the maximum net power output, followed by CO_2/R134a (0.6/0.4), CO_2/R134a (0.85/0.15) and CO_2/R134a (0.4/0.6). However, the maximum net power output was achieved by using CO_2/R134a (0.6/0.4) at a low pressure region. This can be explained by the combination of the following two factors. First, the increase of the mass fraction of R134a leads to lower condensation pressure and results in a higher expansion pressure ratio, which contributes to an increase in expansion power, but also results in the increase of pump power consumption (see Fig. 12(b)). Furthermore, temperature glide in the condensation process increased when mass fraction of R134a increased from 15% to 60%, as shown in Fig. 6. An appropriate temperature glide is beneficial to improve the thermal matching between the working fluid and the cold source. For CO_2/R134a (0.4/0.6), the temperature glide is too large to match the cold source profile and may have caused undesirable fractionating, which is responsible for the expansion power loss [54].

Based on the net power output, the thermal efficiency is defined as:

$$\eta_{th} = \dot{W}_{net,est}/(\dot{Q}_{pre,wf} + \dot{Q}_{gh,wf}) \quad (15)$$

As for the thermal efficiency shown in Fig. 13, CO_2/R134a (0.7/0.3) obtained the maximum thermal efficiency within a range of 8.14–10.35%, followed by CO_2/R134a (0.6/0.4) with 7.84–10.14%, CO_2/R134a (0.85/0.15) with 6.47–10.09%, and CO_2/R134a (0.4/0.6) with 6.09–8.44%. This regularity is quite similar with that of the net power output in the case of high expansion inlet pressure. Looking back at Fig. 10, with the increase of mass fraction of R134a, the total heat recovered from the exhaust gas and engine coolant significantly increased when the expansion inlet pressure was relatively low, but it was not obvious at high pressure. This may explain why CO_2/R134a (0.85/0.15) achieved higher thermal efficiency than CO_2/R134a (0.4/0.6), and why CO_2/R134a (0.7/0.3) performed better than CO_2/R134a (0.6/0.4) at a lower pressure.

For a better understanding of thermal matching in each heat exchangers, exergy analysis was implemented, and that is also provided a guideline to improve this test bench. The irreversible destructions of various heat exchangers and exergy efficiency were calculated by:

$$\dot{I}_{pre} = (\dot{E}_{ec,in} - \dot{E}_{ec,out}) - (\dot{E}_2 - \dot{E}_1) \quad (16)$$

$$\dot{I}_{re} = (\dot{E}_5 - \dot{E}_6) - (\dot{E}_3 - \dot{E}_2) \quad (17)$$

$$\dot{I}_{gh} = (\dot{E}_{g,in} - \dot{E}_{g,out}) - (\dot{E}_4 - \dot{E}_3) \quad (18)$$

$$\dot{I}_{con1+con2} = (\dot{E}_6 - \dot{E}_8) \quad (19)$$

$$\eta_{ex} = \dot{W}_{net,est}/(\dot{E}_{ec,in} - \dot{E}_{ec,out} + \dot{E}_{g,in} - \dot{E}_{g,out}) \quad (20)$$

For the irreversible destruction of heat exchangers shown in Fig. 14, the preheater achieved satisfactory thermal matching with exergy destruction in the range of 0.30–0.73 kW. The gas heater and condensers were the main contributors to the total exergy destruction of system, which are also the main object for modification in upcoming work. This study put more emphasis on analyzing and comparing CO_2/R134a mixtures with various composition ratios. The peak of specific heat, as mentioned earlier, is beneficial to achieve good thermal matching. Based on that, CO_2/R134a (0.4/0.6) had relatively lower exergy destruction in the gas heater. By decreasing the mass fraction of R134a, the exergy destruction in the preheater presented a downward trend and the thermal matching was improved, which is clearly reflected in Fig. 11. Although the pseudocritical temperatures of CO_2/R134a (0.85/0.15), CO_2/R134a (0.7/0.3) and CO_2/R134a (0.6/0.4) all located in the heating process in the regenerator (see Fig. 8), CO_2/R134a (0.7/0.3)

and CO_2/R134a (0.6/0.4) had relatively lower exergy destruction in the regenerator due to their lower heat transfer amount. Note that CO_2/R134a (0.4/0.6) has higher exergy destruction in the condenses compared to the rest of the mixtures. This also validated that the temperature glide of CO_2/R134a (0.4/0.6) is too large to match the cold source, resulting in undesirable irreversible destruction.

Fig. 15 shows exergy efficiencies for various CO_2/R134a mixtures. The regularity of exergy efficiency is similar to that of net power output, which indicates that no sensible change in exergy input was observed among CO_2/R134a mixtures. Maximum exergy efficiency was achieved by maximizing the expansion inlet pressure. Thus, the maximum exergy efficiencies of CO_2/R134a (0.85/0.15), CO_2/R134a (0.7/0.3), CO_2/R134a (0.6/0.4) and CO_2/R134a (0.4/0.6) were 22.82%, 24.90%, 24.34% and 19.52%, respectively. The discussion of exergy destruction can explain the behavior of exergy efficiency.

5. Conclusion

In order to improve cycle performance and alleviate the low-temperature condensation issue encountered with CO_2 in transcritical Rankine cycles (TRC), the CO_2/R134a mixture was presented as working fluid in a TRC test bench to recover waste heat of exhaust gas and engine coolant from a heavy-duty diesel engine. Four CO_2/R134a mixtures with various mass composition ratios, CO_2/R134a (0.85/0.15), CO_2/R134a (0.7/0.3), CO_2/R134a (0.6/0.4) and CO_2/R134a (0.4/0.6), were investigated. The effect of the composition ratio of the CO_2/R134a mixtures on measured operating parameter, heat exchanger performance and cycle performance were discussed. The following conclusions were made:

(1) By increasing the mass fraction of R134a in the CO_2/R134a mixture, the total amount of heat absorption declined, which mainly caused by a decrease in the amount of heat absorption in the regenerator. CO_2/R134a (0.4/0.6) absorbed more heat from the exhaust gas, but less heat from the engine coolant, in comparison with the rest of the mixtures.
(2) For the supercritical CO_2/R134a mixtures, the heat transfer coefficients (HTCs) are in the range of 697.9 ~ 1286.7 W/m^2 °C for the preheater, 115.6 ~ 164.0 W/m^2 °C for the regenerator and 107.6 ~ 111.7 W/m^2 °C for the gas heater. As for the effect of the composition ratio, CO_2/R134a (0.85/0.15) exhibits better heat transfer performance in the preheater, while CO_2/R134a (0.4/0.6) has poor performance in the regenerator. The difference of the HTC in the gas heater is not evident.
(3) With the increase of mass fraction of R134a, the estimation of net power output increases at first, and then decreases. CO_2/R134a (0.7/0.3) obtains the maximum net power output at a high expansion inlet pressure, while CO_2/R134a (0.6/0.4) behaves best at low pressure.
(4) The temperature glide of CO_2/R134a (0.4/0.6) is too large to match cold source profile, leading to undesirable irreversible loss and low exergy efficiency, which is also responsible for the expansion power loss.

CRediT authorship contribution statement

Peng Liu: Conceptualization, Investigation, Visualization, Writing - original draft. **Gequn Shu:** Supervision, Funding acquisition. **Hua Tian:** Writing - review & editing. **Wei Feng:** Writing - review & editing. **Lingfeng Shi:** Investigation. **Xuan Wang:** Investigation.

Declaration of Competing Interest

The authors declare that they have no known competing financial interests or personal relationships that could have appeared to influence the work reported in this paper.

Acknowledgements

The authors would like to acknowledge the National Key Research and Development Plan of China (2017YFE0102800) for grants and supports. The financial support from China Scholarship Council (CSC) to the first author is also gratefully acknowledged.

The U.S. authors recognize Lawrence Berkeley National Laboratory's support from Department of Energy – The United States under Contract No. DE-AC02-05CH11231 and supports from the Energy Foundation. The U.S. Government retains a non-exclusive, paid-up, irrevocable, world-wide license to publish or reproduce the published form of this manuscript, or allow others to do so, for U.S. Government purposes.

References

[1] Lijiang Wei. Experiment research on realizing high proportion of methanol substitution and high efficiency and clean combustion on heavy duty diesel engine. Tianjin university; 2014. Phd thesis.
[2] US-China Clean Energy Research Center. Truck Research Utilizating Collaborative Knowledge Consortium. Available from: http://cerc-truck.anl.gov/.
[3] Liu Peng, Shu Gequn, Tian Hua. How to approach optimal practical Organic Rankine cycle (OP-ORC) by configuration modification for diesel engine waste heat recovery. Energy 2019;174:543–52.
[4] Liu Peng, Shu Gequn, Tian Hua, Wang Xuan, Zhigang Yu. Alkanes based two-stage expansion with interheating Organic Rankine cycle for multi-waste heat recovery of truck diesel engine. Energy 2018;147:337–50.
[5] Zhao Rui, Zhang Hongguang, Song Songsong, Yang Fubin, Hou Xiaochen, Yang Yuxin. Global optimization of the diesel engine–organic Rankine cycle (ORC) combined system based on particle swarm optimizer (PSO). Energy Convers Manage 2018;174:248–59.
[6] Alshammari Fuhaid, Pesyridis Apostolos, Karvountzis-Kontakiotis Apostolos, Franchetti Ben, Pesmazoglou Yagos. Experimental study of a small scale organic Rankine cycle waste heat recovery system for a heavy duty diesel engine with focus on the radial inflow turbine expander performance. Appl Energy 2018;215:543–55.
[7] Delgado. Oscar, Lutsey. Nic, The U.S. SuperTruck Program: Expediting development of advanced HDV efficiency technologies; 2014.
[8] Horst Tilmann Abbe, Rottengruber Hermann Sebastian, Seifert Marco, Ringler Jürgen. Dynamic heat exchanger model for performance prediction and control system design of automotive waste heat recovery systems. Appl Energy 2013;105(1):293–303.
[9] Guillaume L, Legros A, Desideri A, Lemort V. Performance of a radial-inflow turbine integrated in an ORC system and designed for a WHR on truck application: an experimental comparison between R245fa and R1233zd. Appl Energy 2017;186:408–22.
[10] Michael Glensvig, Heimo Schreier, Mauro Tizianel, Helmut Theissl, Peter Krähenbühl, Fabio Cococcetta, and Ivan Calaon, Testing of a Long Haul Demonstrator Vehicle with a Waste Heat Recovery System on Public Road; 2016, SAE International.
[11] Glover Stephen, Douglas Roy, De Rosa Mattia, Zhang Xiaolei, Glover Laura. Simulation of a multiple heat source supercritical ORC (Organic Rankine Cycle) for vehicle waste heat recovery. Energy 2015;93:1568–80.
[12] Yang Min-Hsiung. Optimizations of the waste heat recovery system for a large marine diesel engine based on transcritical Rankine cycle. Energy 2016;113:1109–24.
[13] Yang Min-Hsiung, Yeh Rong-Hua. Economic research of the transcritical Rankine cycle systems to recover waste heat from the marine medium-speed diesel engine. Appl Therm Eng 2017;114:1343–54.
[14] Yağlı Hüseyin, Koç Yıldız, Koç Ali, Görgülü Adnan, Tandiroğlu Ahmet. Parametric optimization and exergetic analysis comparison of subcritical and supercritical organic Rankine cycle (ORC) for biogas fuelled combined heat and power (CHP) engine exhaust gas waste heat. Energy 2016;111:923–32.
[15] Li Chengyu, Wang Huaixin. Power cycles for waste heat recovery from medium to high temperature flue gas sources – from a view of thermodynamic optimization. Appl Energy 2016;180:707–21.
[16] Chen T, Shu G, Tian H, Ma X, Wang Y, Yang H. Compact potential of exhaust heat exchangers for engine waste heat recovery using metal foams. Int J Energy Res 2019.
[17] Grant O. Musgrove., Dereje Shiferaw., Shaun Sullivan., and Lalit Chordia Marc Portnoff. Tutorial: Heat Exchangers for Supercritical CO2 Power Cycle Applications; 2016.
[18] Irwin Levi, Le Moullec Yann. Turbines can use CO_2 to cut CO_2. Science 2017;356(6340):805–6.
[19] Shu G, Shi L, Tian H, Li X, Huang G, Chang L. An improved CO_2-based transcritical Rankine cycle (CTRC) used for engine waste heat recovery. Appl Energy 2016;176:171–82.
[20] Li X, Shu G, Tian H, Shi L, Huang G, Chen T, et al. Preliminary tests on dynamic characteristics of a CO_2 transcritical power cycle using an expansion valve in engine waste heat recovery. Energy 2017;140:696–707.
[21] Wang SS, Wu C, Li J. Exergoeconomic analysis and optimization of single-pressure single-stage and multi-stage CO_2 transcritical power cycles for engine waste heat

recovery: A comparative study. Energy 2018;142:559–77.
[22] Song Jian, Li Xue-song, Ren Xiao-dong, Chun-wei Gu. Performance improvement of a preheating supercritical CO_2 (S-CO_2) cycle based system for engine waste heat recovery. Energy Convers Manage 2018;161:225–33.
[23] Byung Chul Choi. Thermodynamic analysis of a transcritical CO_2 heat recovery system with 2-stage reheat applied to cooling water of internal combustion engine for propulsion of the 6800 TEU container ship. Energy 2016;107:532–41.
[24] Shu G, Long B, Tian H, Wei H, Liang X. Flame temperature theory-based model for evaluation of the flammable zones of hydrocarbon-air-CO < inf > 2 < /inf > mixtures. J Hazard Mater 2015;294:137–44.
[25] Manzolini Giampaolo, Binotti Marco, Bonalumi Davide, Invernizzi Costante, Iora Paolo. CO_2 mixtures as innovative working fluid in power cycles applied to solar plants. Techno-economic assessment. Solar Energy 2019;181:530–44.
[26] Bonalumi D, Lasala S, Macchi E. CO_2-TiCl4 working fluid for high-temperature heat source power cycles and solar application. Renewable Energy 2018.
[27] Wu C, Wang SS, Jiang X, Li J. Thermodynamic analysis and performance optimization of transcritical power cycles using CO_2-based binary zeotropic mixtures as working fluids for geothermal power plants. Appl Therm Eng 2017;115:292–304.
[28] Yin Hebi, Sabau Adrian S, Conklin James C, Mcfarlane Joanna, Lou Qualls A. Mixtures of SF_6 –CO_2 as working fluids for geothermal power plants ☆. Appl Energy 2013;106(11):243–53.
[29] Shu G, Yu Z, Tian H, Liu P, Xu Z. Potential of the transcritical Rankine cycle using CO_2-based binary zeotropic mixtures for engine's waste heat recovery. Energy Convers Manage 2018;174:668–85.
[30] Ge Zhong, Li Jian, Liu Qiang, Duan Yuanyuan, Yang Zhen. Thermodynamic analysis of dual-loop organic Rankine cycle using zeotropic mixtures for internal combustion engine waste heat recovery. Energy Convers Manage 2018;166:201–14.
[31] Dai Baomin, Li Minxia, Ma Yitai. Thermodynamic analysis of carbon dioxide blends with low GWP (global warming potential) working fluids-based transcritical Rankine cycles for low-grade heat energy recovery. Energy 2014;64(1):942–52.
[32] Li Jian, Ge Zhong, Duan Yuanyuan, Yang Zhen. Effects of heat source temperature and mixture composition on the combined superiority of dual-pressure evaporation organic Rankine cycle and zeotropic mixtures. Energy 2019;174:436–49.
[33] Yang MH, Yeh RH. The effects of composition ratios and pressure drops of R245fa/R236fa mixtures on the performance of an organic Rankine cycle system for waste heat recovery. Energy Convers Manage 2018;175:313–26.
[34] Bamorovat Abadi G, Kim KC. Investigation of organic Rankine cycles with zeotropic mixtures as a working fluid: Advantages and issues. Renew Sustain Energy Rev 2017;73:1000–13.
[35] Modi A, Haglind F. A review of recent research on the use of zeotropic mixtures in power generation systems. Energy Convers Manage 2017;138:603–26.
[36] Xi Huan, Li Ming-Jia, He Ya-Ling, Zhang Yu-Wen. Economical evaluation and optimization of organic Rankine cycle with mixture working fluids using R245fa as flame retardant. Appl Therm Eng 2017;113:1056–70.
[37] Chaitanya Prasad GS, Suresh Kumar C, Srinivasa Murthy S, Venkatarathnam G. Performance of an organic Rankine cycle with multicomponent mixtures. Energy 2015;88:690–6.
[38] Bao Junjiang, Zhang Ruixiang, Yuan Tong, Zhang Xiaopeng, Zhang Ning, He Gaohong. A simultaneous approach to optimize the component and composition of zeotropic mixture for power generation systems. Energy Convers Manage 2018;165:354–62.
[39] Magdalena Santos-Rodriguez M, Flores-Tlacuahuac Antonio, Zavala Victor M. A stochastic optimization approach for the design of organic fluid mixtures for low-temperature heat recovery. Appl Energy 2017;198:145–59.
[40] Molina-Thierry David Paul, Flores-Tlacuahuac Antonio. Simultaneous optimal design of organic mixtures and rankine cycles for low-temperature energy recovery. Ind Eng Chem Res 2015;54(13):3367–83.
[41] Pang Kuo-Cheng, Chen Shih-Chi, Hung Tzu-Chen, Feng Yong-Qiang, Yang Shih-Cheng, Wong Kin-Wah, et al. Experimental study on organic Rankine cycle utilizing R245fa, R123 and their mixtures to investigate the maximum power generation from low-grade heat. Energy 2017;133:636–51.
[42] Abadi Gholamreza Bamorovat, Yun Eunkoo, Kim Kyung Chun. Experimental study of a 1 kw organic Rankine cycle with a zeotropic mixture of R245fa/R134a. Energy 2015;93:2363–73.
[43] Wang JL, Zhao L, Wang XD. A comparative study of pure and zeotropic mixtures in low-temperature solar Rankine cycle. Appl Energy 2010;87(11):3366–73.
[44] Jung Hyung Chul, Taylor Leighton. and Susan Krumdieck. An experimental and modelling study of a 1kW organic Rankine cycle unit with mixture working fluid. Energy 2015;81:601–14.
[45] Li Tailu, Zhu Jialing, Wencheng Fu, Kaiyong Hu. Experimental comparison of R245fa and R245fa/R601a for organic Rankine cycle using scroll expander. Int J Energy Res 2015;39(2):202–14.
[46] Wang Y, Liu X, Ding X, Weng Y. Experimental investigation on the performance of ORC power system using zeotropic mixture R601a/R600a. Int J Energy Res 2017;41(5):673–88.
[47] Liu Peng, Shu Gequn, Tian Hua, Feng Wei, Shi Lingfeng, Zhiqiang Xu. Preliminary experimental comparison and feasibility analysis of CO_2/R134a mixture in Organic Rankine Cycle for waste heat recovery from diesel engines. Energy Convers Manage 2019;198:111776.
[48] Wang D, Lu Y, Tao L. Thermodynamic analysis of CO_2 blends with R41 as an azeotropy refrigerant applied in small refrigerated cabinet and heat pump water heater. Appl Therm Eng 2017;125:1490–500.
[49] Wang Enhua, Zhibin Yu, Zhang Hongguang, Yang Fubin. A regenerative supercritical-subcritical dual-loop organic Rankine cycle system for energy recovery from the waste heat of internal combustion engines. Appl Energy 2017;190:574–90.
[50] Kravanja Gregor, Zajc Gašper, Knez Željko, Škerget Mojca, Marčič Simon, Knez Maša H. Heat transfer performance of CO_2, ethane and their azeotropic mixture under supercritical conditions. Energy 2018;152:190–201.
[51] Monjurul Ehsan M, Guan Zhiqiang, Klimenko AY. A comprehensive review on heat transfer and pressure drop characteristics and correlations with supercritical CO_2 under heating and cooling applications. Renew Sustain Energy Rev 2018;92:658–75.
[52] Ma Ting, Chu Wen-xiao, Xiang-yang Xu, Chen Yi-tung, Wang Qiu-wang. An experimental study on heat transfer between supercritical carbon dioxide and water near the pseudo-critical temperature in a double pipe heat exchanger. Int J Heat Mass Transf 2016;93:379–87.
[53] Ahn Yoonhan, Bae Seong Jun, Kim Minseok. Seong Kuk Cho, Seungjoon Baik, Jeong Ik Lee, and Jae Eun Cha. Review of supercritical CO 2 power cycle technology and current status of research and development. Nuclear. Eng Technol 2015;47(6):647–61.
[54] Chys Michael, van den Broek Martijn, Vanslambrouck Bruno, De Paepe Michel. Potential of zeotropic mixtures as working fluids in organic Rankine cycles. Energy 2012;44(1):623–32.